Theoretical and Applied Mechanics Letters 6 (2016) 42–48

Contents lists available at ScienceDirect

Theoretical and Applied Mechanics Letters

journal homepage: www.elsevier.com/locate/taml

Letter

Design of multi-layered porous fibrous metals for optimal sound absorption in the low frequency range

Wenjiong Chen [a], Shutian Liu [a,*], Liyong Tong [b], Sheng Li [a]

[a] State Key Laboratory of Structural Analysis for Industrial Equipment, Dalian University of Technology, Dalian 116023, China

[b] School of Aerospace, Mechanical and Mechatronic Engineering, The University of Sydney, NSW 2006, Australia

HIGHLIGHTS

- A method for enhancing sound absorption coefficient of fibrous metals is presented.
- A fibrous layout with given porosity of multi-layered fibrous metals is suggested.
- Appropriate surface porosity balances dissipation and reflection of acoustic energy.

ARTICLE INFO

Article history:
Received 28 September 2015
Received in revised form
24 December 2015
Accepted 25 December 2015
Available online 21 January 2016
*This article belongs to the Solid Mechanics

Keywords:
Porous fibrous metal
Multi-layer
Low frequency
Acoustic model
Design optimization

ABSTRACT

We present a design method for calculating and optimizing sound absorption coefficient of multi-layered porous fibrous metals (PFM) in the low frequency range. PFM is simplified as an equivalent idealized sheet with all metallic fibers aligned in one direction and distributed in periodic hexagonal patterns. We use a phenomenological model in the literature to investigate the effects of pore geometrical parameters (fiber diameter and gap) on sound absorption performance. The sound absorption coefficient of multi-layered PFMs is calculated using impedance translation theorem. To demonstrate the validity of the present model, we compare the predicted results with the experimental data. With the average sound absorption (low frequency range) as the objective function and the fiber gaps as the design variables, an optimization method for multi-layered fibrous metals is proposed. A new fibrous layout with given porosity of multi-layered fibrous metals is suggested to achieve optimal low frequency sound absorption. The sound absorption coefficient of the optimal multi-layered fibrous metal is higher than the single-layered fibrous metal, and a significant effect of the fibrous material on sound absorption is found due to the surface porosity of the multi-layered fibrous.

As a new type of sound-absorbing materials, porous fibrous metal (PFM), e.g. stainless steel and FeCrAl, has been found to be effective in reducing noise. Compared with the conventional nonmetallic porous fibrous material, PFM becomes attractive due to its mechanical properties, e.g. large surface area, low density, excellent permeability and higher mechanical strength. Hence under extreme circumstances (such as acoustical liner of turbofan engine inlet) PFM may be suitable for applications [1,2]. Therefore recently the study of the sound absorption performance of PFM is of considerable interest.

PFM often has high porosity, as metal fibers cross over each other and there exist a lot of small air passages in the material. Due to these specific pore geometries, energy dissipation in the forms of damping and thermal loss leads to superior sound absorption performance of the PFM. Similar to most sound porous materials, uniform (homogeneous) PFM has excellent sound absorption properties in middle–high frequency range, however, in the low frequency range, the capability of sound absorption is relatively poor. The most common way to improve the performance in low frequencies is to increase the thickness of material [3]. However, this approach may limit the development of PFM to control noise in microelectronics and precision instruments. An alternative way is to optimize the pore geometric parameters to influence the sound propagation in the fibrous material. It has also been found that the gradient porosity can improve PFM's sound absorption performance [1,3–5]. An analysis and design model is in need to be established for designing optimal pore geometric parameter distribution.

* Corresponding author. Tel.: +86 411 84706149; fax: +86 411 84706149.
E-mail address: stliu@dlut.edu.cn (S. Liu).

http://dx.doi.org/10.1016/j.taml.2015.12.002

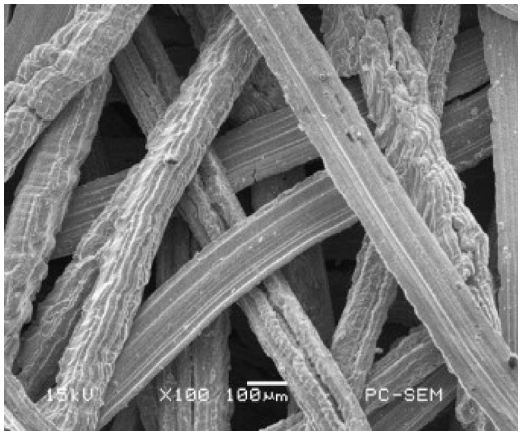

Fig. 1. A typical structural configuration of PFM [12].

Many researchers have studied the acoustic model for predicting the sound absorption properties of uniform porous materials. These models generally fall into two types: empirical and phenomenological models. Bazley and Delany [6] have proposed one of the most representative empirical model. This model can be used to study the single parameter's influence on sound absorption properties, such as state air-flow resistivity, and may not be directly used for studying microscopic structure of porous material. Apart from the empirical model, a number of phenomenological models have also been established, for example, the Biot model [7], Johnson–Champoux–Allard (JCA) model [8,9], Wilson model [10], Lafarge model [11], etc. Accuracy is improved by these models through introducing extra macroscopic acoustic parameters, which are usually obtained through solving the viscous boundary value problems of the pore structure. Relationship of material's sound absorption properties and the pore structure can be established using the JCA model, since it is accurate in both high and low frequencies. Therefore, the JCA model is employed to determine the sound absorption characteristics of PFM in this study.

In this paper, an optimization method of designing multi-layered PFMs is also proposed for maximizing low frequency sound absorption. We use the JCA model to investigate the effects of the pore structural parameters (fiber diameter D and gap w) on sound absorption coefficient. The impedance translation theorem is also introduced to calculate the sound absorption coefficient of multi-layered PFMs. To validate the present analytical model and design method, we compare the obtained results of computation to experimental data available in literature. With the average sound absorption in low frequencies as the objective function and the fiber gaps as the design variables, an optimization method of multi-layered PFMs is established. By using the proposed optimization method, we identified an optimal fiber distribution pattern for optimal sound absorption performance in the low frequency range.

Figure 1 shows a typical structural configuration of PFM [12]. To simplify the calculation, PFM is idealized as a parallel fiber array with repetitive hexagonal distribution patterns of individual fiber having circular cross-section (Fig. 2(a)). Therefore, the parameters of pore structure are only the fiber diameter D and fiber gap w. We perform numerical computations on the scale of the half unit cell (as shown in Fig. 2(b)). The porosity ϕ of the PFM can be conveniently calculated by

$$\phi = 1 - 4\sqrt{3}\pi \left(\frac{D}{2}\right)^2 \Big/ [9(w+D)^2]. \tag{1}$$

In PFM, fibers' density and stiffness are much higher than those of the air in the fibrous material. Therefore, acoustic propagation and dissipation through a rigid frame of porous media can be macroscopically described as a layer of equivalent fluid having the bulk modulus K_{eq} (thermal interaction dependent) and frequency-dependent effective density ρ_{eq} (which is mainly dependent on the viscous interaction between the fluid and frame) [13,14]. In this study, the JCA model [8,9] is employed to calculate the effective density and bulk modulus as

$$\rho_{\mathrm{eq}}(\omega) = \frac{\rho_0 \alpha_\infty}{\phi}\left[1 - \mathrm{j}\frac{\sigma\phi}{\omega\rho_0\alpha_\infty}\sqrt{1 + \mathrm{j}\omega\rho_0\eta\left(\frac{2\alpha_\infty}{\sigma\phi\Lambda}\right)^2}\right], \tag{2}$$

$$\frac{1}{K_{\mathrm{eq}}(\omega)} = \frac{\phi}{\gamma P_0}\left\{\gamma - (\gamma-1)\left[1 - \mathrm{j}\frac{8\eta}{\omega\rho_0 Pr\Lambda'^2} \times \sqrt{1 + \frac{\mathrm{j}\omega\rho_0 Pr}{\eta}\left(\frac{\Lambda'}{4}\right)^2}\right]^{-1}\right\}, \tag{3}$$

where $\mathrm{j} = \sqrt{-1}\rho_0$ and α_∞ denote the fluid density and tortuosity, ϕ the open porosity, σ the static airflow resistivity, ω the angular frequency, η the air viscosity, Λ and Λ' represent the viscous and thermal characteristic lengths respectively, γ the specific heat ratio, P_0 the atmospheric pressure, and Pr is the Prandtl number. The JCA model consists of five macroscopic acoustic parameters: $\phi, \sigma, \alpha_\infty$, Λ and Λ'.

These macroscopic acoustic parameters are determined by the velocity field and property of fluid in fibrous material, which can be defined as

$$\sigma = \frac{\eta}{\phi\langle w_x\rangle}, \tag{4}$$

$$\alpha_\infty = \left\langle E_x^2\right\rangle / \langle E_x\rangle^2, \tag{5}$$

$$\Lambda = \frac{\int_{\Omega_f}|E|^2\,\mathrm{d}V}{\int_{\partial\Omega}|E|^2\,\mathrm{d}S}, \qquad \Lambda' = 2\frac{\int_{\Omega_f}\mathrm{d}V}{\int_{\partial\Omega}\mathrm{d}S}, \tag{6}$$

where the following symbol designates a fluid-phase average

$$\langle * \rangle = \frac{1}{|\Omega_f|}\int_{\Omega_f}(*)\mathrm{d}V \tag{7}$$

and the subscript "x" denote the x component of $*$.

The viscous boundary value problems were solved using finite element analysis at the micro-structure scale under both asymptotic low ($f \to 0$) and high ($f \to \infty$) frequencies, to deduce the macroscopic parameters in the equivalent fluid JCA model [15].

Using the solution of steady state Navier–Stokes (NS) problem, we can deduce the low-frequency limit ($f \to 0$) leading parameter (i.e. the static airflow resistivity σ). The NS problem is defined as

$$\begin{aligned} &\Delta\boldsymbol{w} = \nabla\pi - \boldsymbol{e}, \quad \text{in } \Omega_f, \\ &\nabla\cdot\boldsymbol{w} = 0, \quad \text{in } \Omega_f, \\ &\boldsymbol{w} = \boldsymbol{0}, \quad \text{on } \partial\Omega. \end{aligned} \tag{8}$$

Here, Δ and ∇ represent the local 2-d del and Laplacian differential operators, $\boldsymbol{e}$ is the unit vector, and Ω_f and $\partial\Omega$ denote fluid domain and fluid surface. In addition, $\boldsymbol{w}$ and π represent a static velocity field and associated scalar pressure. As shown in Fig. 3(a), we can numerically (including via the finite element method) solve the velocity field by imposing a no-slip boundary condition at the fluid–solid interface and placing a periodic condition on π and $\boldsymbol{w}$ at the inlet/outlet surfaces. Once we get the solution for a given micro-structure, we can obtain the macroscopic static airflow resistivity by Eq. (4).

Comparing to the pore size, the boundary layer is small under extreme high frequency ($f \to \infty$), so we can ignore its viscous

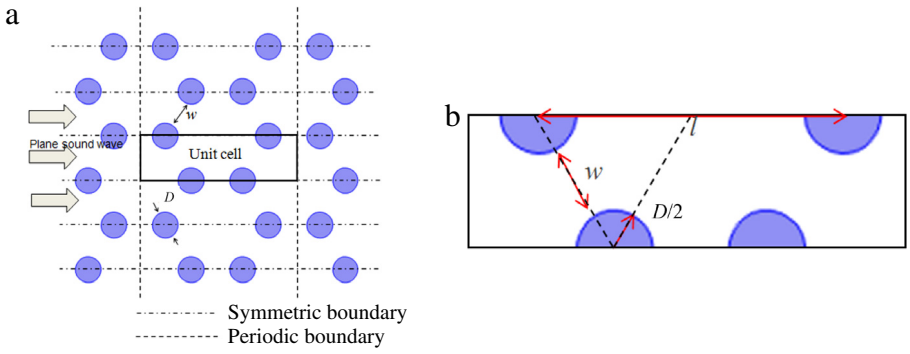

Fig. 2. (a) Cross-sections of parallel fibers array. (b) Periodic micro-structure.

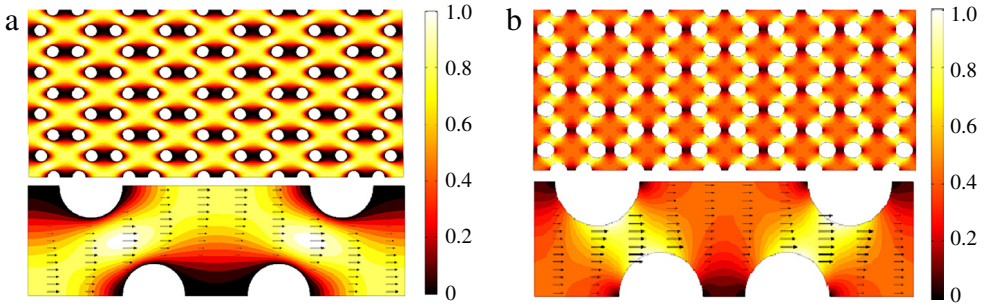

Fig. 3. Velocity field at (a) low-frequency limit ($f \to 0$) and (b) high-frequency limit ($f \to \infty$).

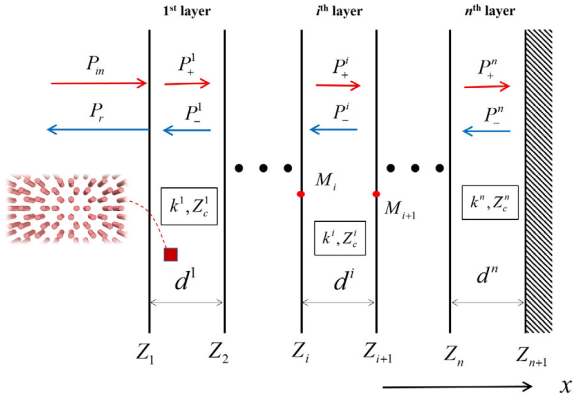

Fig. 4. Sound propagation in a multi-layered PFMs backed by an impervious rigid wall.

effect. Similar to the electric conditions, the governing equations of sound propagation are defined as follows

$$\begin{aligned} &\boldsymbol{E} = -\nabla\Psi + \boldsymbol{e}, \quad \text{in } \Omega_f, \\ &\nabla\boldsymbol{E} = \boldsymbol{0}, \quad \text{in } \Omega_f, \\ &\boldsymbol{E}\cdot\boldsymbol{n} = 0, \quad \text{on } \partial\Omega, \end{aligned} \tag{9}$$

where $\boldsymbol{E}$ and ψ denote the velocity field and pressure (similar to the electric field and electric potential) and $\boldsymbol{n}$ is the outward normal unit vector from the pore boundaries. Again, we can numerically solve the velocity field as shown in Fig. 3(b). When the solution is obtained, we can use Eqs. (5) and (6) to determine the tortuosity α_∞, viscous characteristic length Λ, and thermal characteristic length Λ'.

Table 1 lists properties of the air used in the following simulations.

Consider a multi-layered PFMs sample that is composed of n layers of PFM placed in series format as shown in Fig. 4. In Fig. 4, plane waves propagate in the opposite directions

Table 1
Properties of air used in all studies.

T_0	P_0	ρ_0	η	Pr	γ
291 K	10^5 Pa	1.21 kg/m^3	1.81^{-5} kg/(ms)	0.71	1.4

parallel to the x-axis in the multi-layered PFMs sample backed by an impervious rigid wall. The sound propagation properties of the ith layer PFM are determined by k^i (wave number), Z_c^i (characteristic impedance), and d^i (thickness). The wave number and characteristic impedance can be determined by the effective complex density and the bulk modulus of the ith layer PFM via [14]

$$k^i = \omega\sqrt{\rho_{\text{eq}}^i / K_{\text{eq}}^i}, \qquad Z_c^i = \sqrt{\rho_{\text{eq}}^i K_{\text{eq}}^i}. \tag{10}$$

The governing equation for harmonic plane wave propagation along the x-axis can be expressed as

$$\frac{1}{\rho_{\text{eq}}^i}\frac{\mathrm{d}^2 p^i}{\mathrm{d}x^2} + \omega^2 K_{\text{eq}}^i p^i = 0, \tag{11}$$

where p^i is the sound pressure of the ith layer. Two boundary conditions have to be satisfied at each layer interface: (a) continuity of the sound pressure and (b) continuity of the effective velocity. The solution of Eq. (11) in the ith layer is assumed as a superposition of forward and backward traveling waves

$$p^i(x) = P_+^i \mathrm{e}^{-\mathrm{j}k^i x} + P_-^i \mathrm{e}^{\mathrm{j}k^i x}, \tag{12}$$

where P_+^i and P_-^i are amplitudes of the sound pressure. The effective velocity component can be given, in terms of P_+^i and P_-^i, as

$$v^i(x) = \frac{P_+^i}{Z_c^i}\mathrm{e}^{-\mathrm{j}k^i x} - \frac{P_-^i}{Z_c^i}\mathrm{e}^{\mathrm{j}k^i x}. \tag{13}$$

Table 2
Some PFM samples [3].

Sample number	Fiber diameter D (μm)	Porosity ϕ (%)	Thickness d (mm)
1#	50	73	10
2#	50	91	25
3#	50	85	25
4#	50	80	25

By employing Eqs. (11) and (12) for the pressure and velocity, the impedance Z_i at M_i (i.e. left boundary of the ith layer) is known and can be written as follows

$$Z_i = \frac{p^i(M_i)}{v^i(M_i)} = Z_c^i \frac{P_+ e^{-jk^i x(M_i)} + P_- e^{jk^i x(M_i)}}{P_+ e^{-jk^i x(M_i)} - P_- e^{jk^i x(M_i)}}. \quad (14)$$

At M_{i+1} (i.e. right boundary of the ith layer), the impedance Z_{i+1} is given by

$$Z_{i+1} = \frac{p^i(M_{i+1})}{v^i(M_{i+1})} = Z_c^i \frac{P_+ e^{-jk^i x(M_{i+1})} + P_- e^{jk^i x(M_{i+1})}}{P_+ e^{-jk^i x(M_{i+1})} - P_- e^{jk^i x(M_{i+1})}}. \quad (15)$$

From Eq. (15), it follows that

$$\frac{P_-^i}{P_+^i} = \frac{Z_{i+1} - Z_c^i}{Z_{i+1} - Z_c^i} e^{-2jk^i x(M_{i+1})}. \quad (16)$$

Substitution of Eq. (16) into Eq. (14), the impedance translation theorem can be obtained

$$Z_i = Z_c^i \frac{-jZ_{i+1} \cot g\left(k^i d^i\right) + Z_c^i}{Z_{i+1} - jZ_c \cot g\left(k^i d^i\right)}. \quad (17)$$

As the multi-layered PFMs sample backed by an impervious rigid wall, the impedance at the surface of the wall is infinite. Then, by using Eq. (17), the total impedance at the surface of the multi-layered fibrous metal Z_1 can be calculated. Therefore, the reflection coefficient of the multi-layered PFMs' surface can be determined as follows

$$R_1 = \left(Z_1 - Z_c'\right) / \left(Z_1 + Z_c'\right), \quad (18)$$

where Z_c' is the characteristic impedance of air. The sound absorption coefficient of multi-layered fibrous material can be written as

$$\alpha = 1 - |R_1|^2. \quad (19)$$

PFM's sound absorption coefficient is calculated using an idealized and simplified hexagonal pore structure, and this pore structure and fibrous distribution are indeed different from the real PFM. In order to prove the validity of the proposed theoretical model for single- and multi-layered PFMs, we compare the present theoretical results with the experimental ones in Refs. [1,3]. Four PFM samples and their geometric parameters are listed in Table 2. The samples all have the same diameter 50 μm, but different thickness (10–25 mm) and porosities (73%–91%). As reported in Refs. [1,3], these four PFM samples were used in different assembling sequences to form four types of single- and multiple-layered porous structures as given in Table 3, which were tested for the measurement of sound absorption coefficient. The tested structures A and B are the single-layered PFM with PFM samples 1# and 2# respectively, structure C is composed of three layers of PFM in the order of PFM samples 2#, 3# and 4#, and structure D is composed of two layers with PFM samples 4# and 2#.

Comparisons between the obtained results of the proposed model and experimental measurements are shown in Figs. 5 and 6 for single- and multi-layered PFMs, respectively. Figure 5 shows that the predicted sound absorption coefficients for structures A and B (e.g. single-layered PFM) match well with the measured ones

Table 3
Four tested structures (the first layer is referred to the one that is closest to the incident sound resource (see Fig. 4)).

	A Ref. [1]	B Ref. [1]	C Ref. [3]	D Ref. [3]
First layer	1#	2#	2#	4#
Second layer	–	–	3#	2#
Third layer	–	–	4#	–

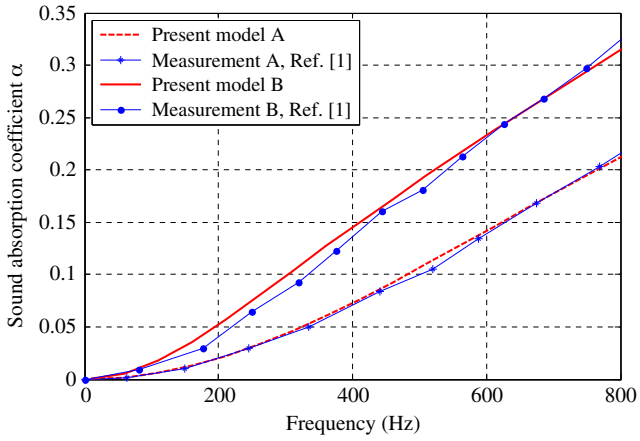

Fig. 5. Sound absorption coefficient predicted and measured for single-layered PFM A and B.

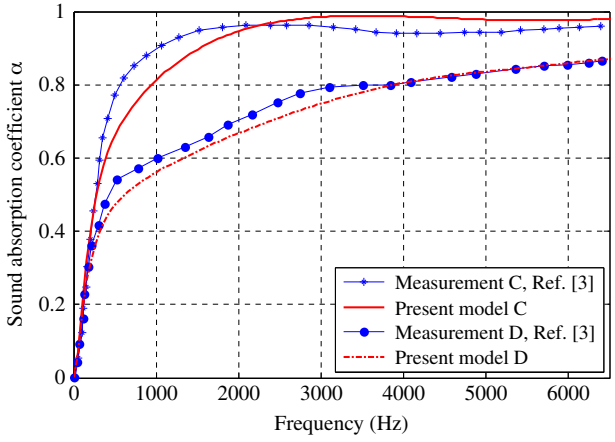

Fig. 6. Sound absorption coefficient predicted and measured for multi-layered PFMs C and D.

in the low frequency range. For structures C and D (e.g. multi-layered PFMs), there exists a small deviation between the computations and measurements as shown in Fig. 6. This small deviation may be due to the idealized and simplified hexagonal pore structure and the simplified treatment of the transmission between the layers in our theoretical model or the inevitable micro-defects in the test samples.

We consider the optimum design of the pore structures (i.e. fiber diameter and gap) of multi-layered PFMs for enhancing the performance of sound absorption in the low frequency range. From the previous work [16], we can know that variation of fiber

Table 4
The calculated macroscopic parameters and performance index of optimal four-layer PFMs (the first layer is referred to the one that is closest to the incident sound resource).

	Fiber diameter D (μm)	Fiber gap w (μm)	Porosity ϕ (%)	Thickness (mm)	Performance index I
First layer	50	40	81.3%	12.5	0.358
Second layer	50	88	92.1%	12.5	
Third layer	50	75	90.3%	12.5	
Fourth layer	50	64	88.4%	12.5	

gap can easily affect the sound absorption but fiber diameter's change cannot. Therefore we choose the fiber gaps in each layer are the design variables, and keep the fiber diameter fixed as 50 μm. The optimization model for maximizing the average sound absorption in the low frequency range (<500 Hz) is formulated as follows

$$\begin{aligned} &\text{Find:} && \boldsymbol{X} = (w_1, w_2, \ldots, w_n)^{\mathrm{T}}, \\ &\text{Maximize:} && I(\boldsymbol{X}) = \frac{1}{N}\sum_{i=1}^{N}\alpha(f_i), \\ &\text{Subject to:} && w_{\min} < w < w_{\max}, \\ & && \sum_{i}^{n} d^i = L_0, \\ & && 10 \le f_i < 500 \text{ Hz}, \end{aligned} \tag{20}$$

where n is number of layers, I denotes the average sound absorption coefficient index, L_0 is the absorber thickness (in this paper, we choose the thickness of absorber is 50 mm), $\alpha(f_i)$ denotes the normal sound absorption coefficient computed at the ith frequency, and N is the number of discrete frequencies in frequency range of interest (here, we choose $N = 50$ and the frequency interval $\Delta f = f_{i+1} - f_i = 10$ Hz). We can use the finite difference method to derive the sensitivity of the objective function I to the design variables w_i as

$$\frac{\partial I}{\partial w_i} = \frac{I(w_i + \Delta w) - I(w_i)}{\Delta w}. \tag{21}$$

Sequential linear programming (SLP) is used to solve the optimization problem Eq. (20).

A single-layered PFM with thickness of 50 mm and diameter of 50 μm backed with a rigid wall is considered. The sound absorption index I in the low frequency range as a function of fiber gap w is calculated by using parameter analysis and is shown in Fig. 7. In Fig. 7, it is found that there exists a specific value of fiber gap (i.e. $w = 52$ μm) where we can achieve the optimal sound absorption performance index (i.e. $I = 0.301$). The corresponding sound absorption coefficient for optimal single-layered fibrous material (as a function of frequency) is shown in Fig. 8.

We aim to investigate the optimal fiber gaps of four-layer PFMs (Fig. 9(a)) for maximizing the sound absorption performance index I in the low frequency range. The thickness of material is 50 mm (same as single-layered PFM), and each layer has the same thickness 12.5 mm. The diameter is also chosen as 50 μm. By solving the optimization problem Eq. (20), the optimal fiber gap distribution is achieved. The optimal fiber gaps from first layer to fourth layer are $w_1 = 40$ μm, $w_2 = 88$ μm, $w_3 = 75$ μm, and $w_4 = 64$ μm, respectively. The corresponding porosities are 81.3%, 92.1%, 90.3%, 88.4%. Figure 9(b) shows the iteration history of the objective function and Fig. 9(c)–(f) depict the sketches of pore structures of each layer. In this case, the optimal sound absorption performance index I is 0.358, which represents a 19.3% increase when compared with single-layered fibrous material with the same diameter and thickness. The calculated macroscopic parameters and performance index are presented in Table 4. Figure 10 shows the sound absorption coefficient of optimal single and four-layer PFMs in the low frequency range (10–500 Hz).

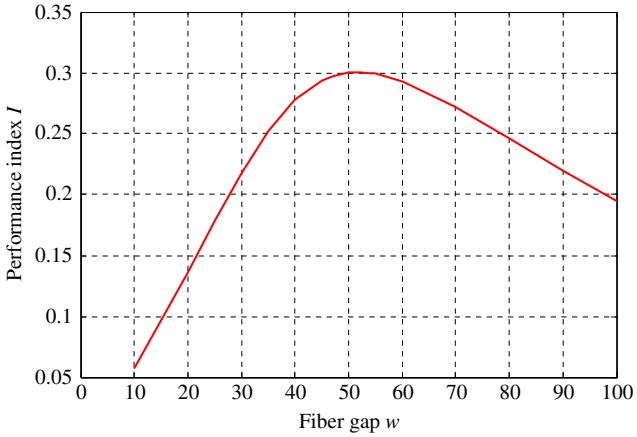

Fig. 7. The sound absorption index I in the low frequency range as a function of fiber gap w.

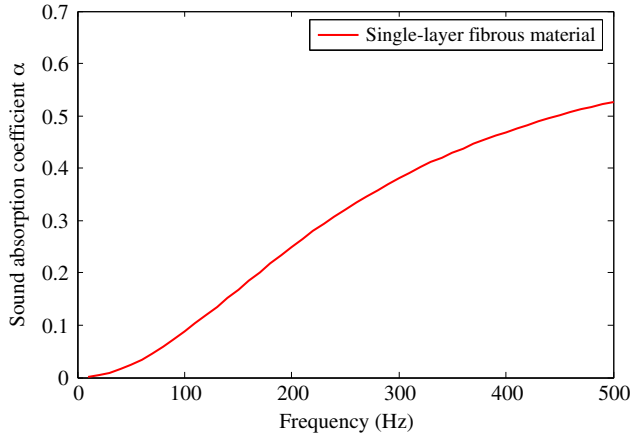

Fig. 8. The sound absorption coefficient of optimal design of single-layered fibrous material.

It can be seen from Table 4 that the fiber gaps (or porosities) decrease along the sound incident direction except for the first layer in the low frequency range. To understand the effects of the first layer (surface pore structure) on the sound absorption performance of multi-layered fibrous metals, we perform a parametric study by considering the same multi-layered materials in Table 4 but with four different fiber gaps in the first layer. The different fiber gap in the first layer is chosen as 40 μm, 20 μm, 80 μm, 100 μm (i.e. porosities are 81.4%, 69.1%, 91.1%, 93.3%, respectively) while the other three layers are the same as fibrous metals in Table 4. These four cases with different fiber gaps in the first layer are denoted as S1, S2, S3, S4, respectively.

To compare the sound performances of these four multi-layered structures, the average sound absorption coefficient index defined in Eq. (20) will be used. Table 5 presents the average sound absorption coefficient indexes of the four multi-layered structures in both low and mid-high frequency ranges. For the case in the low frequency range (10–500 Hz), case S1 has the optimal

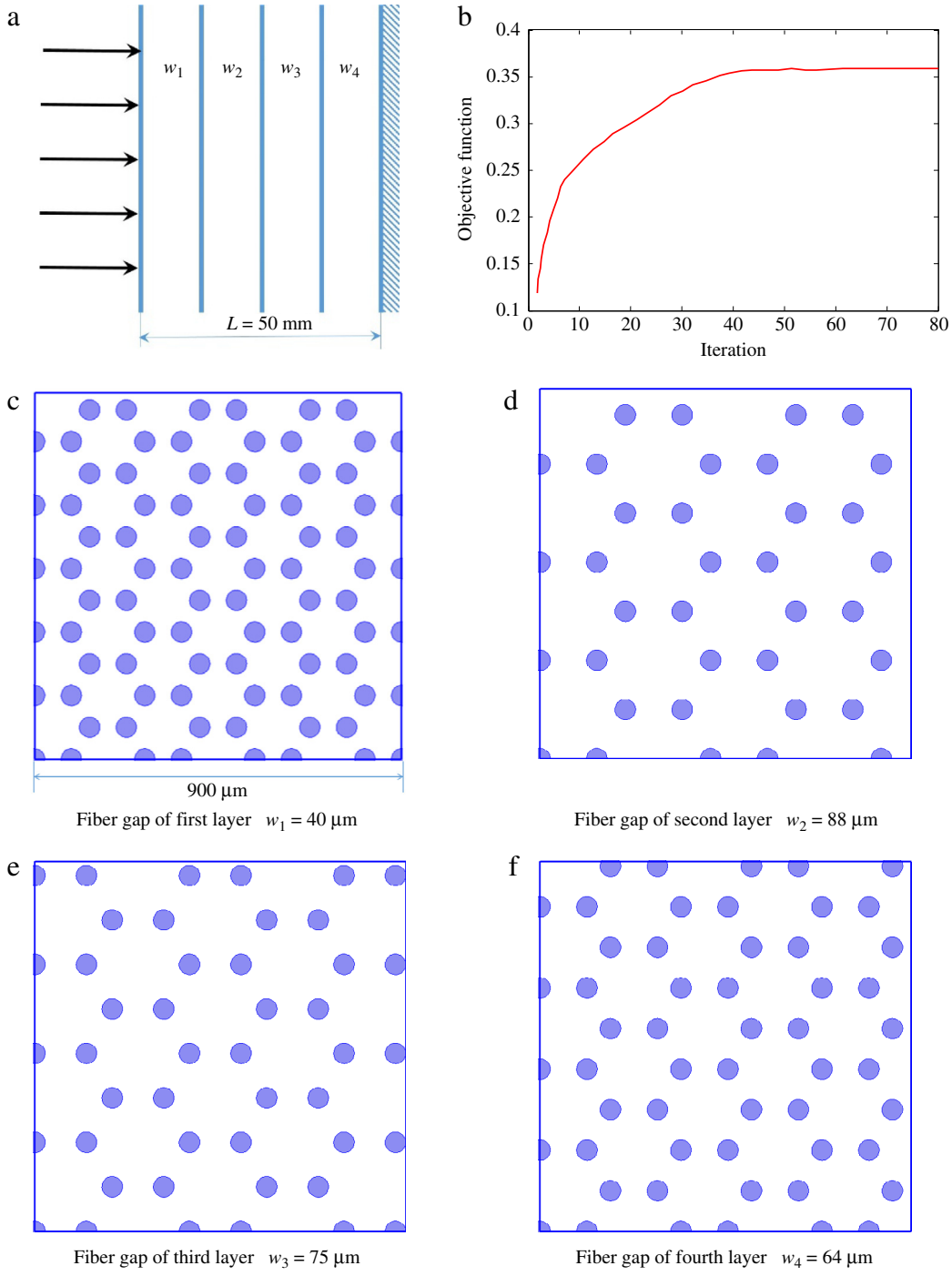

Fig. 9. (a) Four-layer PFMs backed a rigid wall. (b) Iteration history of objective function. Optimal fiber gaps of each layer: (c) first layer; (d) second layer; (e) third layer; (f) fourth layer.

sound absorption performance. For the mid-high frequency range (500–5000 Hz), cases S3 and S4 have better sound absorption performances than S1. The detail sound absorption coefficient curves of the four multi-layered structures are present in Fig. 11. It is obvious that the sound absorption coefficient of the multi-layered PFMs increases with the frequency generally. It can also be noted that: (a) the sound absorption coefficient for case S2 with the lowest surface porosity is higher than other cases when the frequency is below about 130 Hz; (b) case S1 has the largest sound absorption coefficient when the frequency is in the range of 130–500 Hz; (c) the absorption coefficient increases monotonically with the surface porosity when frequency is above ∼1500 Hz. It is believed that the acoustic resistance plays a major role for sound absorption in the low frequency range due to that a smaller surface porosity yields a higher acoustic resistance [14]. Although more acoustic energy can be dissipated by a higher acoustic resistance in porous media, most of acoustic energy is reflected when the surface porosity is too small. Therefore, an appropriate surface porosity of multi-layered PFMs can balance the dissipation and reflection of acoustic energy to maximize the sound absorption.

From Table 5 and Fig. 11, it can be seen that the variation of the surface porosity has a significant effect on the sound

Table 5
The average sound absorption coefficient indexes of S1–S4.

Frequency range	Average sound absorption coefficient index			
	S1	S2	S3	S4
10–500 Hz	0.358	0.213	0.262	0.234
500–5000 Hz	0.774	0.441	0.934	0.934

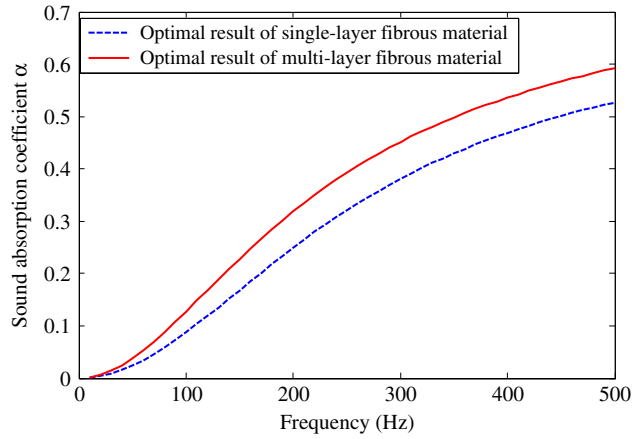

Fig. 10. The sound absorption coefficient of optimal single and four-layer PFMs.

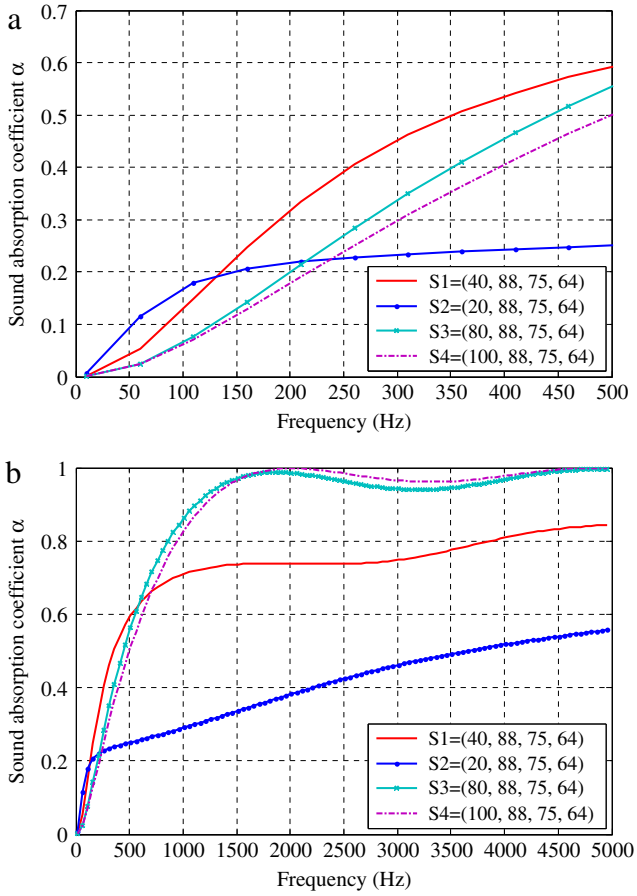

Fig. 11. Sound absorption coefficient of four multi-layered PFMs with different fiber gaps of first layer. (a) 10–500 Hz; (b) 10–5000 Hz.

absorption of multi-layered fibrous structures. Generally speaking, an arrangement in the order of high porosity to low porosity along the sound incident direction is beneficial for improving the sound absorption in mid-high frequency range. However, this rule of porosity distribution cannot apply to low frequency range.

In this paper, an analytical model and a design method for multi-layered PFMs are presented for improving low frequency sound absorption. In the analysis model, the PFM is idealized and simplified as a periodic hexagonal arrangement of fibers aligned in one direction, and the sound absorption coefficient is determined based on the JCA acoustic model and impedance translation theorem; In the optimization model, the average sound absorption coefficient at low frequencies is chosen as the objective function and the fiber gaps as the design variables. Comparing the predicted results with experimental data in the literature verifies that the analytical model is valid and effective. Numerical examples demonstrate also that the optimization model is applicable and efficient. The average sound absorption coefficient of optimal four-layered PFMs is 20% higher than that of the single-layered PFM with the same diameter and thickness in the low frequency range. Furthermore, the surface porosity of the multi-layered PFMs has a significant influence on the fibrous material's sound absorption. Generally, increasing the surface porosity can improve sound absorption in mid-high frequency range but does not work for the low frequency range. The work presented in this paper would provide the references and guides for the future studies and manufacture of multi-layered PFMs.

Acknowledgments

The authors acknowledge the support of the National Basic Research Program (973 Program) of China (2011CB610304), the National Natural Science Foundation of China (11332004 and 11402046), China Postdoctoral Science Foundation (2015M571296), the 111 Project (B14013) and the CATIC Industrial Production Projects (CXY2013DLLG32).

References

[1] H. Meng, Q. Ao, H. Tang, et al., Dynamic flow resistivity based model for sound absorption of multi-layer sintered fibrous metals, Sci. China Technol. Sci. 57 (2014) 2096–2105.
[2] B Zhang, T.N. Chen, Calculation of sound absorption characteristics of porous sintered fiber metal, Appl. Acoust. 70 (2009) 337–346.
[3] H.P. Tang, J.L. Zhu, Y. Ge, et al., Sound absorbing characteristics of fibrous porous materials gradient structure, Rare Metal Mater. Eng. 36 (2007) 2220.
[4] K. Huang, D.H. Yang, S.Y. He, et al., Acoustic absorption properties of open-cell Al alloy foams with graded pore size, J. Phys. D: Appl. Phys. 44 (2011) 365405.
[5] J.E. Lefebvre, V. Zhang, J. Gazalet, et al., Acoustic wave propagation in continuous functionally graded plates: an extension of the Legendre polynomial approach, IEEE Trans. Ultrason. Ferroelectr. Freq. Control 48 (2001) 1332–1340.
[6] M. Delany, E. Bazley, Acoustical properties of fibrous absorbent materials, Appl. Acoust. 3 (1970) 105–116.
[7] M.A. Biot, Theory of propagation of elastic waves in a fluid-saturated porous solid. I. Low-frequency range, J. Acoust. Soc. Am. 28 (1956) 168–178.
[8] D.L. Johnson, J. Koplik, R. Dashen, Theory of dynamic permeability and tortuosity in fluid-saturated porous media, J. Fluid Mech. 176 (1987) 379–402.
[9] Y. Champoux, J.F. Allard, Dynamic tortuosity and bulk modulus in air-saturated porous media, J. Appl. Phys. 70 (1991) 1975–1979.
[10] D.K. Wilson, Relaxation-matched modeling of propagation through porous media, including fractal pore structure, J. Acoust. Soc. Am. 94 (1993) 1136–1145.
[11] D. Lafarge, P. Lemarinier, J.F. Allard, et al., Dynamic compressibility of air in porous structures at audible frequencies, J. Acoust. Soc. Am. 102 (1997) 1995–2006.
[12] W. Zhou, Y. Tang, M. Pan, et al., Experimental investigation on uniaxial tensile properties of high-porosity metal fiber sintered sheet, Mater. Sci. Eng. A 525 (2009) 133–137.
[13] R.F. Lambert, Propagation of sound in highly porous open-cell elastic foams, J. Acoust. Soc. Am. 73 (1983) 1131–1138.
[14] J. Allard, N. Atalla, Propagation of Sound in Porous Media: Modelling Sound Absorbing Materials 2e, John Wiley & Sons, 2009.
[15] C. Perrot, F. Chevillotte, R. Panneton, Dynamic viscous permeability of an open-cell aluminum foam: Computations versus experiments, J. Appl. Phys. 103 (2008) 024909.
[16] S. Liu, W. Chen, Y. Zhang, Design optimization of porous fibrous material for maximizing absorption of sounds under set frequency bands, Appl. Acoust. 76 (2014) 319–328.